Aerospace Science and Technology 168 (2026) 110983

Contents lists available at ScienceDirect

Aerospace Science and Technology

journal homepage: www.elsevier.com/locate/aescte

Structural damage diagnosis and prognosis with fleet digital twin considering similarity of individual structural features

Jiaqi Xu [a,b], Dingqiang Dai [a,b], Xuan Zhou [a,b,*], Marco Giglio [c], Claudio Sbarufatti [c], Leiting Dong [a,b,*]

[a] School of Aeronautic Science and Engineering, Beihang University, Xueyuan Road 37, Haidian, 100191, Beijing, China
[b] Tianmushan Laboratory, Shuanghongqiao Street 166, Hangzhou, 310023, Zhejiang, China
[c] Department of Mechanical Engineering, Politecnico di Milano, Via La Masa 1, Milano, 20156, Milano, Italy

ARTICLE INFO

Jae-Hung Han

Keywords:
Damage diagnosis and prognosis
Copula function
Physics-decoded variational neural Network
Digital twin
Fleet maintaenance

ABSTRACT

Diagnosis and prognosis of the structural health state based on online monitoring data is crucial for enabling condition-based maintenance and ensuring the safety of aeronautical structures. However, most existing studies focus on structural damage diagnosis and prognosis at the individual level, often overlooking the potential of utilizing fleet-wide data, which requires accurately measuring the similarity between structures and the correlation of damage states across individuals in the fleet. To address this, we propose a novel method for fleet-level structural damage diagnosis and prognosis that leverages the similarity of individual structural features. The method introduces a Physics-Decoded Variational Neural Network, enabling accurate extraction of structural features as well as quantifying damage. Additionally, a copula function is used to model the joint probability distribution of damage states across different structures, based on structural feature similarity metrics. This approach allows for collaborative updating of damage states across the fleet using observations from individual structures during the diagnosis process. Validation on a typical damaged aeronautical panel demonstrates that the proposed method achieves more accurate diagnosis and prognosis of individual structural damage states within a fleet, while reducing uncertainties during service compared to conventional individual-based approaches. This method shows promise for integration into a fleet-level airframe digital twin framework, advancing the implementation of condition-based maintenance across fleets.

1. Introduction

In aeronautical structures, cyclic loads experienced during flight can lead to crack initiation and growth in critical regions, significantly compromising the structural integrity of the aircraft [1,2]. Variations in service load histories and manufacturing processes result in different damage states among aircrafts within the fleet [3,4]. Consequently, the conventional approach with uniform service life and periodic inspections has become increasingly inadequate for ensuring in-service safety. This highlights the urgent need for Condition-Based Maintenance (CBM) [5,6].

In recent years, the concept of the Airframe Digital Twin (ADT) [7,8] has gained significant attention in the aerospace field due to its potential for real-time damage diagnosis and prognosis. By integrating predictive models with real-time monitoring data [9,10], the ADT enables accurate tracking of structural damage evolution [7,11,12]. Furthermore, it facilitates the continuous updating of model parameters to reduce prediction uncertainties, thereby supporting dynamic CBM decision-making [13–15].

Bayesian-based approaches, such as the extended Kalman filter [16], particle filter (PF) [17,18], have been widely applied in ADT systems due to there capability to effectively model crack growth processes under both epistemic and aleatoric uncertainties [17,19]. For instance, Li et al. [17] utilized a dynamic Bayesian network-based digital twin to construct a probabilistic model for diagnosing and prognosing fatigue crack growth in aircraft wings. Similarly, Ye et al. [20] developed a reconfigurable PF model for constructing digital twins of structures with multiple damage modes. Wang et al. [21] proposed a weighted adaptive Kalman filtering-based method to fuse guided wave and strain signals, achieving high-accuracy monitoring of hole-edge crack propagation. Their work emphasize Bayesian-based approaches as key tools for damage diagnosis and prognosis in aeronautical structures.

However, current Bayesian-based digital twin methods predominantly focus on individual structural damage diagnosis and prognosis.

* Corresponding authors.
E-mail addresses: zhoux@buaa.edu.cn (X. Zhou), ltdong@buaa.edu.cn (L. Dong).

https://doi.org/10.1016/j.ast.2025.110983
Received 11 January 2025; Received in revised form 6 September 2025; Accepted 20 September 2025
Available online 28 September 2025

These methods primarily update the damage state of a specific structure using inspection data from the corresponding individual [16,22,23], with limited consideration of fleet-level applications. In reality, the damage states of multiple individuals within a fleet are interrelated, despite inherent differences. A straightforward approach to address this would involve considering the damage states of all structures in the fleet and constructing a comprehensive diagnosis and prognosis model [24]. But, as the number of individuals in the fleet increases, this approach faces the challenge of dimensional catastrophe, with computational complexity and storage requirements rising rapidly. Consequently, for digital twins in fleet maintenance, it is essential to develop effective methods that balance the differences and similarities in fleet damage states, enabling efficient utilization of monitoring data for collaborative diagnosis. This optimization is crucial for reducing costs and improving efficiency in fleet maintenance. Nonetheless, two major challenges must be addressed to achieve this goal.

The first key challenge is accurately quantifying the similarities between different individuals within the fleet. These similarities primarily lie in the geometric and material properties of the structures, which should be precisely identified. Moreover, variations in these properties often result in differences in structural monitoring signals [25]. However, conventional health monitoring methods typically establish a direct relationship between monitoring signals and damage states, often neglecting the influence of structural differences [23]. To address this limitation, the Physics-Decoded Variational Neural Network (PDVNN) [26] proposed by the authors, integrates a reduced-order model encompassing damage states and individual structural features into its decoder. By embedding physics-based knowledge related to structural damage into the monitoring signal-based damage quantification process, PDVNN enables the simultaneous and probabilistic identification of both damage states and individual structural features.

After determining individual structural features and quantifying their similarity, the second key challenge is enabling collaborative structural damage diagnosis and prognosis across the fleet based on these similarities. When two structures exhibit similarity, their damage states are expected to follow a joint probability distribution with a degree of correlation [27]. By observing one structure, this joint distribution can be updated to synchronize the damage states of both structures. The difficulty in constructing this joint distribution lies in effectively describing the dependence between the damage size distributions of different structures. The copula function provides a robust approach by decomposing the joint distribution of multiple random variables into their marginal distributions and the dependence structure between them [28]. This separation allows independent modeling of marginal distributions and dependence structures, making it a versatile tool widely applied in fields such as financial asset modeling [29], consumer behavior analysis [30], supply chain risk management [31], and multivariate reliability analysis [32–34]. This decomposition framework offers valuable insights for constructing the joint distribution of damage states using the similarity metrics derived from the PDVNN.

In summary, the main contribution of this study is the development of a method to extract features and quantify similarity metrics of different individuals within a fleet using the proposed PDVNN. Additionally, a joint distribution of damage states across different structures is established based on the copula function. The collaborative update of damage states for multiple structures is then achieved within the PF framework. The effectiveness of the proposed method in enhancing the accuracy of structural damage diagnosis and reducing uncertainties throughout the process is demonstrated through a case study of a typical damaged aeronautical panel.

The remainder of this paper is organized as follows: Section 2 presents the proposed framework for structural damage diagnosis and prognosis in a fleet considering individual structural features. Section 3 describes validation on aeronautical panels of a helicopter, including the test setup, numerical modeling, parameter settings, and comparison methods. Section 4 provides a comparison and discussion of the results, highlighting the advantages of the proposed method in structural damage diagnosis and prognosis. Finally, Section 5 concludes the paper and explores potential directions for future research.

2. Structural damage diagnosis and prognosis in fleet considering individual structural features

This section provides a detailed description of the proposed method for structural damage diagnosis and prognosis in a fleet considering individual structural features, as illustrated in Fig. 1. Section 2.1 begins with an overview of the conventional PF-based approach to structural damage diagnosis and prognosis, which forms the foundation of the proposed method. Section 2.2 explains how damage states and structural features are extracted using the PDVNN, which serves as the input for Section 2.3, where the joint distribution of damage states across structures in the fleet is modeled using a copula function. Finally, Section 2.4 integrates these methods into a framework for collaborative structural damage diagnosis and prognosis, leveraging SHM signals from different individuals to update the damage states across the entire fleet.

2.1. Particle filter for structural damage diagnosis and prognosis

In this section, we first introduce PF-based methods for structural damage diagnosis and prognosis. For the structural damage diagnosis and prognosis problem, the system state is represented by the crack length **a**. In the crack growth process, the crack growth rate $\frac{\mathrm{d}\mathbf{a}}{\mathrm{d}N}$ can

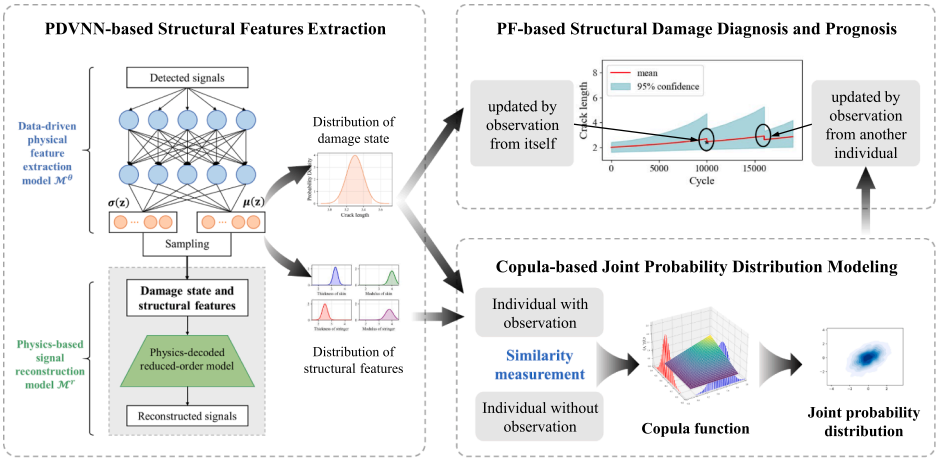

Fig. 1. Structure damage diagnosis and prognosis in a fleet considering individual structural features.

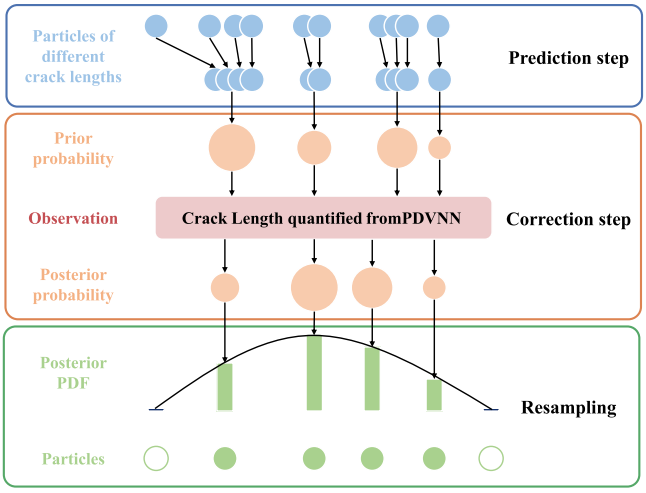

Fig. 2. Prediction and correction steps in the particle filter with embedded PDVNN.

be described as:

$$\frac{\mathrm{d}\mathbf{a}}{\mathrm{d}N} = f(\Delta\mathbf{K}, \mathbf{a}; \boldsymbol{\mu}) \tag{1}$$

where, $\Delta\mathbf{K}$ is the Stress Intensity Factor (SIF) range and $\boldsymbol{\mu}$ is uncertainty parameters related to the crack growth process.

Appending the parameter $\boldsymbol{\mu}$ and the crack length $\mathbf{a}$ gives the augmented state vector $\mathbf{x} = [\mathbf{a}, \boldsymbol{\mu}]$, then the state transfer equation of the system can be described as [14,17,22]:

$$\mathbf{x}_k = \begin{bmatrix} \mathbf{a}_k \\ \boldsymbol{\mu}_k \end{bmatrix} = \begin{bmatrix} \mathbf{a}_{k-1} + e^{\omega_{\mathbf{a},k}} f(\Delta\mathbf{K}, \mathbf{a}; \boldsymbol{\mu})\Delta N \\ \boldsymbol{\mu}_{k-1} + \omega_{\boldsymbol{\mu},k} \end{bmatrix} \tag{2}$$

where $\mathbf{x}_k$ represents the state vector at time step k. The evolution model includes $\omega_{\boldsymbol{\mu},k}$, the crack extension noise following a Gaussian distribution $N\left(-\frac{\sigma_\omega^2}{2}, \sigma_\omega^2\right)$ satisfying $\mathbb{E}\left(e^{\omega_{\mathbf{a},k}}\right) = 1$, and $\omega_{\boldsymbol{\mu},k}$, the parameter evolution noise.

The observation model is given by:

$$\mathbf{y}_k = \mathbf{a}_k + \boldsymbol{\eta}_k \tag{3}$$

where $\mathbf{y}_k$ is the observation of crack length and $\boldsymbol{\eta}_k$ is the measurement noiseobeying a zero-mean Gaussian distribution.

In the Bayesian framework, the unknown state vector $\mathbf{x}_k$ at step k is inferred based on the following sequence of observations, as shown in Fig. 2:

1) For the prediction step is performed, the state vector $\mathbf{x}_k$ at step k is predicted based on the state variable $\mathbf{x}_{k-1}$ at the previous time step and the state transfer between two neighboring time steps.

$$p(\mathbf{x}_k \mid \mathbf{y}_{1:k-1}) = \int p(\mathbf{x}_k \mid \mathbf{x}_{k-1}) p(\mathbf{x}_{k-1} \mid \mathbf{y}_{1:k-1}) \mathrm{d}\mathbf{x}_{k-1} \tag{4}$$

2) For the correction step, the joint probability distribution $p(\mathbf{x}_k \mid \mathbf{x}_{1:k})$ of the state variable $\mathbf{y}_{1:k}$ is updated when the observatioin $\mathbf{y}_{1:k}$ is acquired:

$$p(\mathbf{x}_k \mid \mathbf{y}_{1:k}) = \frac{p(\mathbf{y}_k \mid \mathbf{x}_k) p(\mathbf{x}_k \mid \mathbf{y}_{1:k-1})}{p(\mathbf{y}_k \mid \mathbf{y}_{1:k-1})} \tag{5}$$

where $p(\mathbf{y}_k \mid \mathbf{x}_k)$ is the observed likelihood function, and $p(\mathbf{y}_k \mid \mathbf{y}_{1:k-1})$ is the normalization constant.

Practicle problems often correspond to nonlinear non-Gaussian systems and Eqs. (4) and (5) are difficult to compute analytically. In the PF, N_s particles are used to represent $p(\mathbf{x}_k \mid \mathbf{y}_{1:k})$ and their approximate solutions are obtained using Sequential Importance Resampling (SIR):

$$p(\mathbf{x}_k \mid \mathbf{y}_{1:k}) \approx \sum_{i=1}^{N_s} \tilde{\omega}_k^{(i)} \delta\left(\mathbf{x}_k - \mathbf{x}_k^{(i)}\right) \tag{6}$$

where N_s is the number of particles, $\delta(\cdot)$ is the Dirac delta function, $\mathbf{x}_k^{(i)}$ is the i_{th} particle, and $\tilde{\omega}_k^{(i)}$ is the weight of the i_{th} sample. More details on the PF-based methods for structural damage diagnosis and prognosis can be found in Ref. [14].

2.2. Extracting individual structural features using physics-decoded variational neural network

This section describes the process of extracting individual features of different structures within a fleet using the previously proposed PDVNN. These individual feature parameters are denoted as $\boldsymbol{\Lambda}$ in this study. In the PDVNN framework, these parameters, along with the structural damage states, are extracted based on the signal inputs from structural health monitoring (SHM) systems. The network architecture of the PDVNN, shown in Fig. 3, comprises a data-driven physical feature extraction model, a physics-decoded reduced-order model, and latent variables that connect these models.

1) **Data-Driven Physical Feature Extraction Model ($\mathcal{M}^\theta$):** represented by the left part of the architecture, this model is parameterized by θ. It accepts the detected signals $\mathbf{x}$ as input and outputs the latent variables corresponding to physical features.

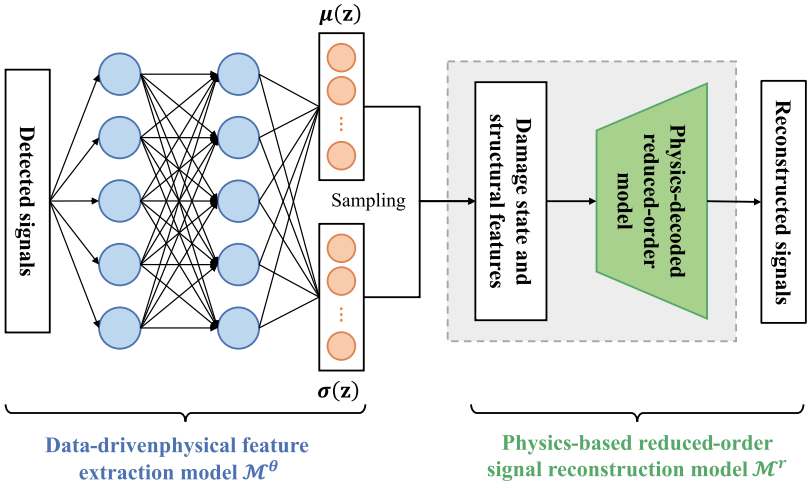

Fig. 3. Architectures of PDVNN for structural feature extraction.

2) **Latent Variable Representation:**the middle part of the PDVNN represents the physical features, $\mathbf{z} = [\mathbf{a}, \mathbf{\Lambda}]$, where $\mathbf{a}$ denotes the damage state parameters and $\mathbf{\Lambda}$ corresponds to the structural features. These latent variables are probabilistically modeled with their mean $\boldsymbol{\mu}(\mathbf{z})$ and standard deviation $\boldsymbol{\sigma}(\mathbf{z})$, enabling uncertainty quantification.
3) **Physics-based Reduced-order Signal Reconstruction Model ($\mathcal{M}^r$):** the right part of the PDVNN integrates the physics-based reduced-order model, which is built based on the full-order simulation of the damage structures. It reconstructs the sensor signals $\hat{\mathbf{x}}$ using the sampled latent variables as input, thereby enabling a closed-loop process for validation and refinement.

The variational inference method within a Bayesian framework [35] is employed to train the PDVNN, and the loss function $\mathcal{L}$ can be represented as:

$$\mathcal{L} = \mathbb{E}_{q_\phi(\mathbf{z}|\mathbf{x})}\left[\log p_\theta(\mathbf{x}|\mathbf{z})\right] - \mathrm{KL}\left(q_\phi(\mathbf{z}|\mathbf{x})\|p(\mathbf{z})\right) \tag{7}$$

where the first term $\mathbb{E}_{q_\phi(\mathbf{z}|\mathbf{x})}\left[\log p_\theta(\mathbf{x}|\mathbf{z})\right]$ represents the expected log-likelihood of the data under the variational posterior and $\mathrm{KL}\left(q_\phi(\mathbf{z}|\mathbf{x})\|p(\mathbf{z})\right)$ is the KL divergence between the variational posterior $q_\phi(\mathbf{z}|\mathbf{x})$ parameterized by ϕ and the prior $p(\mathbf{z})$. More details can be found in Ref. [21].

Once the PDVNN is effectively trained, it can recognize the damage states and structural features of individual structures based on SHM monitoring signals, while quantifying the associated uncertainties. The damage states are used to update individual damage states during the PF process described in Section 2.1, while the structural features are utilized to assess the correlation of damage states among individuals in Section 2.3.

2.3. Copula-based collaborative measurement between individuals

In this section, the Copula function is adopted to establish a similarity measure between different individuals based on the structural features obtained in Section 2.2, and to derive the joint probability distribution of their damage states, as shown in Fig. 4. Copulas are multivariate cumulative distribution functions [36,37] with uniform marginal distributions on the interval [0,1]. They allow the dependence structure between random variables to be decoupled from their marginal distributions, enabling fleet-level correlation modeling while maintaining independent modeling of individual distributions. This property makes Copulas particularly suitable for collaborative structural damage diagnosis and prognosis. In this study, the Frank Copula function is used, as it effectively captures symmetric correlations and is well-suitable for data without significant tail dependence, which aligns with the distribution characteristics of structural damage data. Its cumulative distribution function is defined as:

$$C_\theta^{\mathrm{Frank}}(u_1, u_2) = -\frac{1}{\theta}\log\left[1 + \frac{\left(e^{-\theta u_1} - 1\right)\left(e^{-\theta u_2} - 1\right)}{\left(e^{-\theta} - 1\right)}\right] \tag{8}$$

where u_1 and u_2 are the Cumulative Distribution Functions (CDFs) of the crack length distributions of the two structures, and θ is the correlation parameter. In this study, θ is estimated based on the similarity of the distributions of structural feature distributions d_λ and the similarity of predicted crack length distributions d_a.

To quantify the similarity between two distributions, the Kullback-Leibler (KL) divergence [38,39]is adopted, which measures the discrepancy between two probability density functions $p(\mathbf{x})$ and $q(\mathbf{x})$, and is defined as:

$$D_{KL}(P \,||\, Q) = \int p(\mathbf{x}) \log \frac{p(\mathbf{x})}{q(\mathbf{x})} \mathrm{d}\mathbf{x} \tag{9}$$

where P and Q denote the target and reference distributions, respectively. By definition, $D_{KL}(P \,||\, Q) = 0$ when the two distributions are identical, and increases as the discrepancy grows.

A simple heuristic method is then used to convert the KL divergence measure into the following similarity measure. The basic idea is that the greater the similarity between the distributions of two individuals, the higher the correlation coefficient. Conversely, when the damage states of the two individuals differ more significantly, the correlation coefficient should decrease accordingly. Based on this concept, the conversion formula is given as follows:

$$\theta = \theta_0 \times \left(d_0 - d_\Lambda\right)\left(1 - S\left(d_a\right)\right) \tag{10}$$

where, θ_0 and d_0 are hyperparameters to tune, and the Sigmoid function

$$S\left(d_a\right) = \frac{1}{1 + e^{-d_a'}} \tag{11}$$

is used to process d_a. Because $d_a > 0$, it is shifted to the left direction and normalized as d_a', thereby converting it to the range [0, 1]. Due to

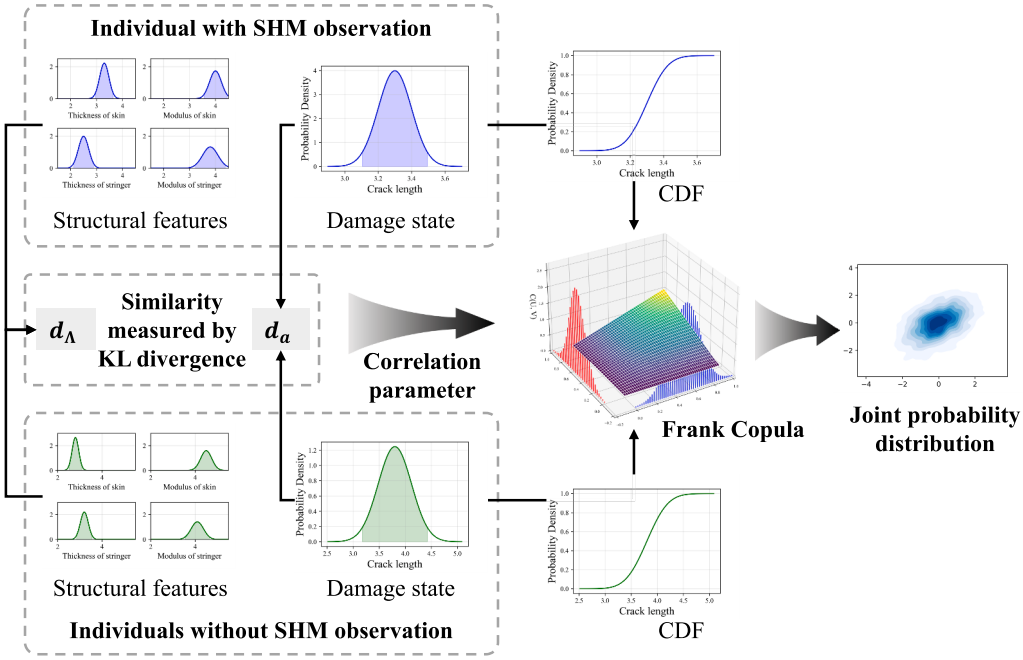

Fig. 4. Copula-based joint distribution modeling between individuals.

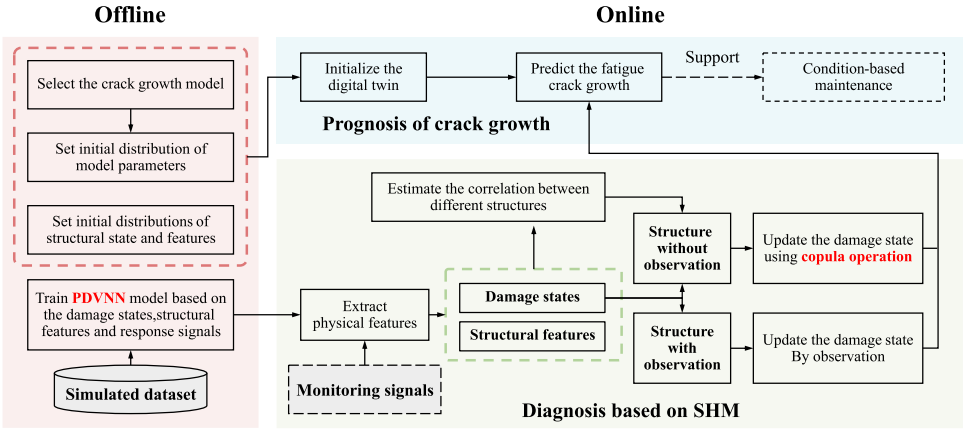

Fig. 5. The Framework of the collaborative diagnosis and prognosis in a fleet.

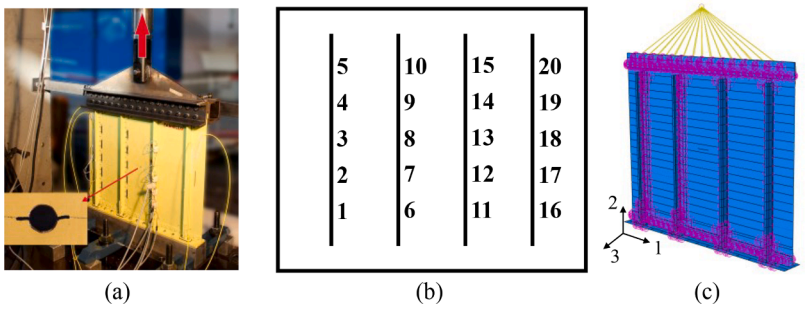

Fig. 6. Experiment and simulation of the fuselage panel. (a) The experiment setup, (b) Sensor positions and labels, and (c) The numerical model.

the properties of the Sigmoid function, when d_a becomes very large—indicating that the predicted damage distributions of the two structures are very different—the term associated with it in Eq. (10) will tend to zero.

Furthermore, to prevent erroneous updates caused by weak correlations, a trigger threshold should be introduced. The correlation parameter in copula functions corresponds directly to Kendall's /tau [40]. For Frank Copula functions, the correspondence is as follows:

$$\tau(\theta) = 1 - \frac{4}{\theta}\left[1 - D_1(\theta)\right] \tag{12}$$

where $D_k(x)$ is the Debye function, defined for any positive integer k as

$$D_k(x) = \frac{k}{x^k}\int_0^x \frac{t^k}{e^t - 1}\mathrm{d}t \tag{13}$$

It is generally accepted that $|\tau| > 0.6$ indicates a strong correlation, as indicated in [40]. Therefore, the corresponding Copula parameter is approximately $\theta \approx 5.7$, which is adopted in this study as the threshold for enabling collaborative updates. If the estimated correlation is below this threshold, no update is performed to avoid potential negative effects on prediction accuracy.

Based on the approach, the joint distribution of damage states between different individuals within a fleet can be modeled to support collaborative structural damage diagnosis and prognosis.

2.4. Collaborative structural damage diagnosis and prognosis in a fleet

In this section, the structural feature extraction, joint distribution modeling and the PF are integrated into a framework for the collaborative structural damage diagnosis and prognosis in a fleet, as illustrated in Fig. 5.

In the offline phase, the feature extraction model in the PDVNN is trained using a simulated dataset generated from the simulation of damaged structures. This training supports online SHM. The prior distributions of crack lengths, structural features, and crack growth model parameters are then used to initialize M individual digital twins within the fleet, forming the initial fleet digital twin.

In the online phase, the crack growth for each individual structure is continuously predicted probabilistically based on the load history accumulated throughout the fleet's service life, which served as the basis of condition-based maintenance. When monitoring data becomes available for the individual M_A within the fleet, the monitoring signal is first fed into the physical feature extraction model $\mathcal{M}^\theta$ to quantify both the crack length distribution and the structural feature distribution for that individual. The quantified crack lengths are then used to update the distributions of uncertain parameters, evaluate particle weights, and generate new particles, similar to conventional individual-based PF. Meanwhile, the structural feature distributions are temporarily stored for subsequent correlation analysis between individuals.

Meanwhile, for the individual M_B for which no monitoring data are available, the Frank Copula function is employed to approximate the joint distribution $p(a_A, a_B)$ of crack lengths from the individual M_A and the individual M_B. Where, the expression of the Frank Copula function is determined by the correlation parameter θ, which is obtained by the KL dispersion measure of the damage state and structural features obtained from the aforementioned monitoring data and the sign extraction model $\mathcal{M}^\theta$ based on the transformation of Eq. (3). Subsequently, the joint distribution $p(a_A, a_B)$ is updated based on the monitoring results of individual M_A.Then, the updated marginal distribution of the crack lengths in individual M_B is extracted from the updated $p(a_A, a_B)$, which forms the new particles of the individual M_B.

3. Validation of the proposed framework on damaged aeronautical panels

This section validates the proposed framework for structural damage diagnosis and prognosis using a set of damaged aeronautical=

panels. Section 3.1 provides an overview of the aeronautical panels, detailing the fatigue experiment setup and the numerical model employed. Section 3.2 focuses on the generation of the simulated dataset used for training the PDVNN model, along with the construction of the experimental dataset. Section 3.3 describes the implementation of the method, including the selection of relevant parameters. Finally, Section 3.4 presents a comparison between the proposed framework and a conventional individual-based PF-based structural damage diagnosis and prognosis approach, along with an introduction to the performance evaluation metrics.

3.1. Helicopter fuselage panel and its numerical model

The skin of the panel has dimensions of 600 mm in width, 500 mm in height, and 0.81 mm in thickness, and is fabricated from Al 2024 alloy. Four L-shaped stringers, each 435 mm in length and 1.2 mm in thickness, are constructed from Al 7075 alloy and are spaced 150 mm apart on the skin's surface. The fatigue crack growth tests were conducted as shown in Fig. 6(a). The specimen is equipped with 20 Fiber Bragg Grating (FBG) sensors, strategically arranged along the rivet line to measure static strain at peak load, as depicted in Fig. 6(b). An initial 16 mm of damage is introduced at the center of the panel and the specimen is then subjected to sinusoidal loading with a maximum load amplitude $F_{\max} = 35\text{kN}$ and a stress ratio of $R = 0.1$ [41].

A finite element model was created to simulate the response of the damaged structure under the applied loading conditions, as shown in Fig. 6(c). In the model, shell elements are used to represent the skin and stringers, while triaxial springs model the rivets, with each stringer connected to the skin by rivets [42].

For the fatigue crack growth, Paris law [43] is employed to describe the growth process:

$$\frac{\mathrm{d}a}{\mathrm{d}N} = C(\Delta K)^m \tag{14}$$

where a is the half crack length, N is the number of load cycles, ΔK is the SIF range, C and m are unkown material parameters. According to Ref. [44], the SIF range, ΔK, is calculated as follows:

$$\Delta K = \beta \Delta\sigma \sqrt{\pi a} \tag{15}$$

where β is the geometry factor and $\Delta\sigma$ is the far-field stress range.

β is a function of the structure's geometry and the relative crack length. When the structure is determined, it can be expressed as $\beta(a)$, with empirical expressions available in Ref. [44]. As shown in Fig. 7, the relationship between β and the relative crack length a/b (b is the spacing between the centerlines of two adjacent stringers) is affected by the stringer stiffness μ. It is defined as:

$$\mu = \frac{w t_s E_s}{w t_s E_s + b t_p E_p} \tag{16}$$

where w is the stringer width, t_s and t_p are the thickness of the stringer and skin, respectively, and E_s and E_p are the Young's modulus of the stringer and skin, respectively. In this study, w and b are considered accurate, while t_s, t_p, E_s and E_p may deviate from their nominal values and are quantified using the PDVNN.

By fitting a polynomial and interpolating the $a/b - \beta$ curves from Ref. [44], the relationship between β and the a/b can be derived for any given stringer stiffness μ. Since the growth range of the unilateral crack is constrained, only the relevant portion of the curve is utilized in the fitting process to reduce the order of the polynomial while preserving accuracy.

3.2. Experimental and simulated dataset

In this study, a simulated dataset is generated to train the PDVNN model, whereas the experimental dataset is employed to validate the performance of the proposed method.

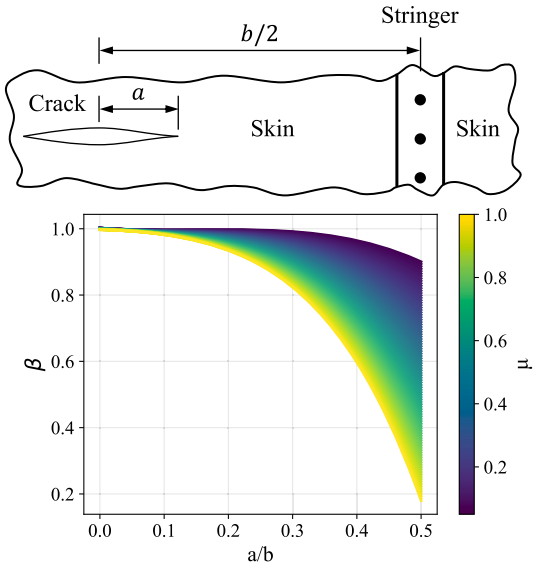

Fig. 7. Effect of stringer stiffness on relationship between β and relative crack length a/b.

Table 1
Distribution range of structural features.

Parameter	Meaning	Nominal value	Range
t_p	Skin's thickness	0.80 [mm]	0.78~0.82 [mm]
t_s	Stringer's thickness	1.30 [mm]	1.25~1.33 [mm]
E_p	Skin's Young's modulus	73.8 [GPa]	73.0~75.0 [GPa]
E_s	Stringer's Young's modulus	70.3 [GPa]	69.1~71.5 [GPa]

The experimental dataset is presented first. Fatigue crack growth data were collected from three specimens, labeled #1, #2, and #3. The crack growth process for these panels is depicted in Fig. 8(a). For these specimens, 9, 12, and 10 measurements were recorded, respectively, including strain measurements and corresponding crack lengths captured by 20 FBG sensors. To mitigate the influence of load variations on strain measurements during the fatigue crack growth process, a damage index based on monitoring signals was introduced [45,46]. Assuming that N_s strain sensors were arranged along the rivet line to measure the static strain at peak load, the normalized damage index ϵ_k^{norm} for the k_{th} sensor is defined as:

$$\epsilon_k^{\text{norm}} = \frac{\epsilon_k}{\sum_{i=1}^{N_s} \frac{\epsilon_i}{N_s}} \tag{17}$$

The experimental dataset is thus defined as:

$$\mathcal{D}_{\text{panel}}^{\text{exp}} = \left\{ \mathbf{a}_i, \boldsymbol{\epsilon}_i^{\text{norm}} \right\} \tag{18}$$

where $i = 1, 2, 3$ corresponds to the experiments of the three specimens, $\mathbf{a}_i$ represents the i_{th} specimen, and $\boldsymbol{\epsilon}_i^{\text{norm}}$ is the set of damage indices of the i_{th} specimen.

Then, the simulated dataset to train the PDVNN model is presented. After evaluating the influence of various parameters on the simulation results, the geometric dimensions and material properties of the connectors for the upper and lower parts of the specimen were fixed. Structural features closely related to crack growth, such as the properties of the skin and stringer, were identified as key features. The types and ranges of these structural features are summarized in Table 1.

Therefore, the set of structural features of the specimen $\boldsymbol{\Lambda}_{\text{panel}}^{\text{sim}}$ consists of the following four parameters:

$$\boldsymbol{\Lambda}_{\text{panel}}^{\text{sim}} = \left\{ t_p, t_s, E_p, E_s \right\} \tag{19}$$

Using Eqs. (15) and (15), each set of parameters determines the value of the SIF for a specimen at a given crack size. The process of generating

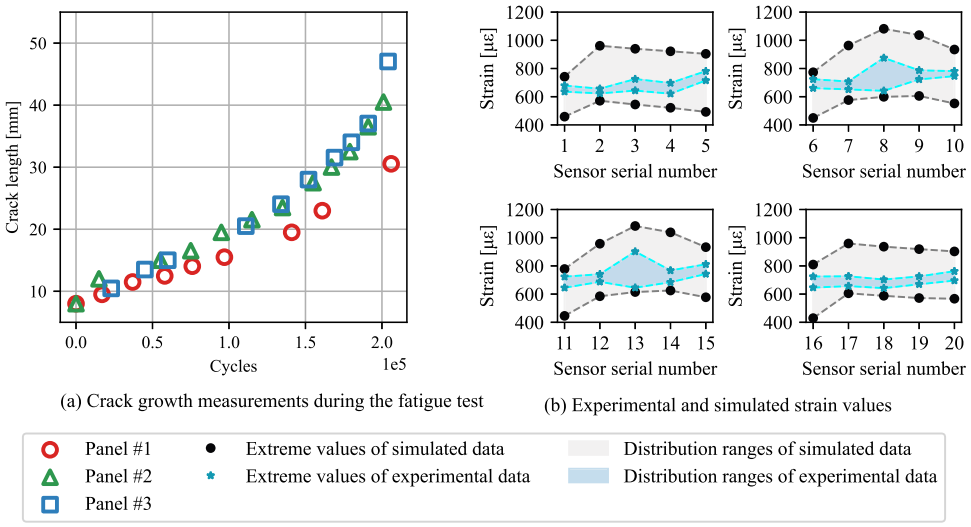

(a) Crack growth measurements during the fatigue test (b) Experimental and simulated strain values

Fig. 8. (a) Crack growth experiments during the three fatigue tests, (b) Experimental and simulated strain ranges of 20 FBG sensors.

the simulated dataset involves Latin hypercube sampling, parametric modeling and automated simulation. This process yields a final dataset containing 2000 samples. More details are provided in Ref. [26]. The generated simulation dataset is defined as:

$$\mathcal{D}_{\text{panel}}^{\text{sim}} = \left\{ \mathbf{a}_{\text{panel}}^{\text{sim}}, \mathbf{\Lambda}_{\text{panel}}^{\text{sim}}, \boldsymbol{\varepsilon}_{\text{panel}}^{\text{sim}} \right\} \tag{20}$$

where $\mathbf{a}_{\text{panel}}^{\text{sim}}$ represents the sampled crack size and $\boldsymbol{\varepsilon}_{\text{panel}}^{\text{sim}}$ denotes the corresponding strain values at the sensor locations within the simulation model.

The ranges of simulated and measured strains at the 20 measurement points are shown in Fig. 8(b). It is clear that the strain range of the simulated dataset $\mathcal{D}_{\text{panel}}^{\text{sim}}$ encompasses the strain range of the experimental dataset $\mathcal{D}_{\text{panel}}^{\text{exp}}$. This comprehensive coverage of strain range is essential for the structural feature quantification, as it ensures that the calibration process primarily relies on interpolation rather than extrapolation.

Based on the realistic operational characteristics of the aircraft fleet, a sufficiently large sample set is necessary for more comprehensive validating of the proposed approach. Due to practical limitations such as long test cycles and high costs, it is challenging to verify the method using large-scale experimental data or in-service structures. Therefore, a hypothetical dataset of 36 panels was generated to emulate fleet-level variability.

To characterize variations among individual aircraft, reasonable variations in geometric dimensions, material properties, and crack propagation model parameters were introduced into the simulation model. Generate a hypothetical dataset following the same procedure used to create the simulated dataset, defined as:

$$\mathcal{D}_{\text{panel}}^{\text{hyp}} = \left\{ \mathbf{a}_{\text{panel}}^{\text{hyp}}, \mathbf{\Lambda}_{\text{panel}}^{\text{hyp}}, \boldsymbol{\varepsilon}_{\text{panel}}^{\text{hyp}} \right\} \tag{21}$$

where $\mathbf{a}_{\text{panel}}^{\text{hyp}}$ represents the sampled crack size, $\mathbf{\Lambda}_{\text{panel}}^{\text{hyp}}$ consists of the same key features as Eq. (19), and $\boldsymbol{\varepsilon}_{\text{panel}}^{\text{hyp}}$ denotes the corresponding strain values at the sensor locations within the simulation model.

To mimic real-world monitoring environments, noise was added to the simulated strain signals. This large-scale, high-fidelity dataset was subsequently used to validate the proposed methodology. Relevant parameter settings are provided in the Appendix A.

3.3. PDVNN training and parameter setting of the proposed method

In this study, a PDVNN model was constructed to extract damage states and structural features of specimens using the simulated dataset $\mathcal{D}_{\text{panel}}^{\text{sim}}$.

Table 2
Hyperparameter setting for PDVNN training.

Parameter	Setting
Learning rate scheduler	Cosine learning rate from 0.03 to 0.0005
Epochs	5000
Batch size	64
Activation	Sigmoid

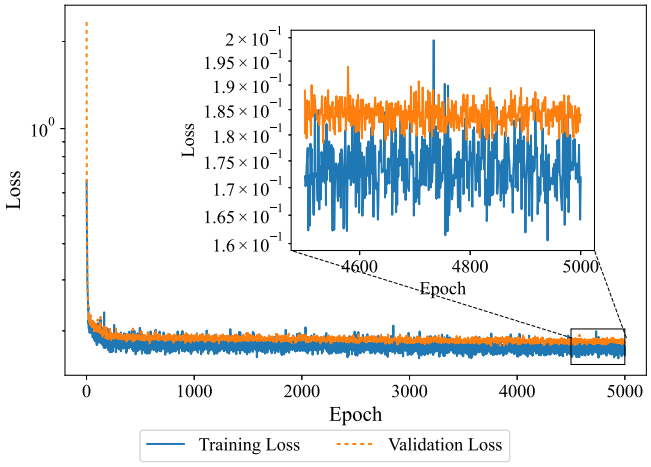

Fig. 9. PDVNN training process.

First, a neural network was used to pre-train the physics-decoded reduced-order model $\mathcal{M}^r$. The input size of this network is 5, representing the damage state and structural features, while the output size is 20, corresponding to the number of FBG sensors. The pre-trained neural network consists of two hidden layers with 7 and 23 neurons, respectively.

Subsequently, the physics-decoded reduced-order model, $\mathcal{M}^r$, was integrated into the PDVNN framework. The physical feature extraction model $\mathcal{M}^\theta$ in the PDVNN also consists of two hidden layers, with 21 and 11 neurons, respectively. The model has an opposite input-output structure compared to the pre-trained reduced-order model.

For training the PDVNN model, the simulated dataset $\mathcal{D}_{\text{panel}}^{\text{sim}}$ was divided into training and validation subsets with an 0.8/0.2 ratio. The network was optimized using the Adam optimizer, with

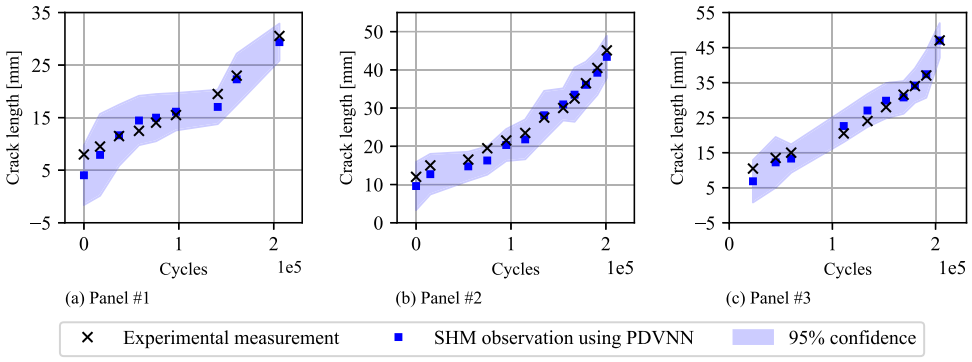

Fig. 10. Quantification of the crack size during the fatigue crack growth by PDVNN.

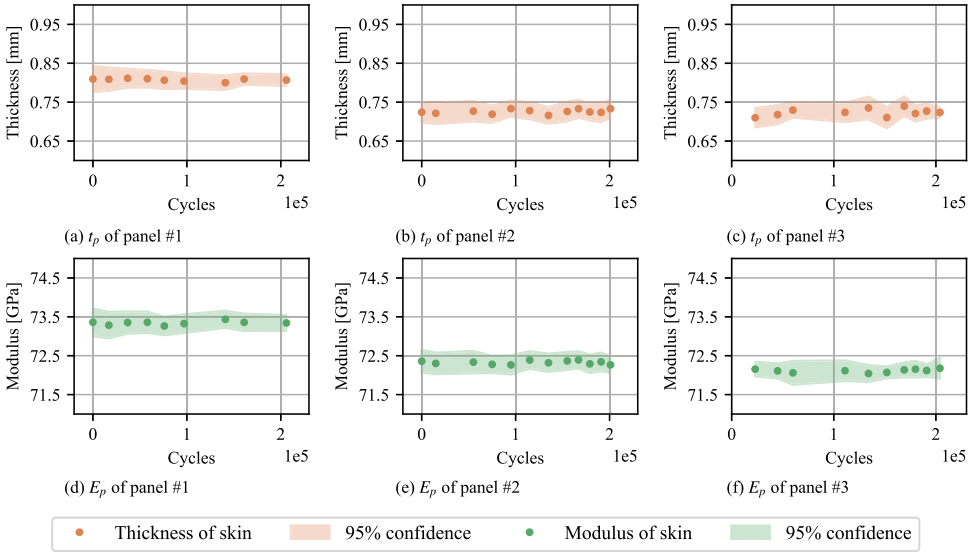

Fig. 11. Quantification of structural features of skin during fatigue crack growth.

Table 3
Parameter setting for particle filter.

Parameters	Meaning	Value
a_0	Prior distribution of the initial half crack length	$N \sim (8.00, 1.00^2)$
$\log C_0$	Prior distribution of $\log C$	$N \sim (-10.72, 0.20^2)$
m_0	Prior distribution of m	$N \sim (2.69, 0.08^2)$
$\Delta\sigma$	Stress range	45
ω_a	Noise of the crack growth	$N \sim (-0.05^2/2, 0.05^2)$
ω_1	Noise in the evolution of $\log C$ and m	$N \sim (0, 0.01^2)$
ω_2	Noise in the evolution of t_s, E_s, t_p, E_p	$N \sim (0, 0.01^2)$
N_s	Number of particles	1000
ΔN	Increment of loading cycle	1000
θ_0	Hyperparameters for the correlation metric	30
d_0	Hyperparameters for the correlation metric	0.33

hyperparameters specified in Table 2. To mitigate overfitting, early stopping was employed during training.

The training and validation losses are shown in Fig. 9. The results demonstrate that the training loss consistently remained lower than the validation loss, with the gap between them being within an acceptable range. This indicates effective model learning and good generalization performance on unseen data.

The parameter setting of the PF and the correlation measurement method are listed in Table 1. Prior distribution of the structural features t_s, E_s, t_p, E_p is the same as that in Table 3.

3.4. Methods for comparison and rvaluation of model accuracy and precision

In this study, the proposed method, which integrates the PDVNN and Copula function, is compared with the conventional individual-based PF algorithm. In the individual-based PF method [13,14], monitoring signals are utilized exclusively within individual samples, without considering the similarities in damage states and structural features across different individuals in the fleet.

To evaluate the accuracy and precision of the methods, several metrics are employed. The root mean square error (RMSE) and correlation index (R^2) are used to assess the model's prediction error and its ability to fit the observations. RMSE ranges from [0,∞), with 0 indicating a perfect fit, while R^2 ranges from [0,1], with an ideal value of 1 indicating perfect correlation.

Additionally, the average band width (ABW) of the prediction intervals is used to evaluate the model's prediction accuracy. ABW represents the average bandwidth of the prediction interval, calculated as the difference between the upper and lower prediction limits for each observation. A narrower bandwidth is desirable, with an ideal value of 0 signifying deterministic predictions without uncertainty [47].

The three metrics can be calculated as follows:

$$\mathrm{RMSE} = \sqrt{\frac{1}{n}\sum_{i=1}^{n}\left(y_i - \hat{y}_i\right)^2} \tag{22}$$

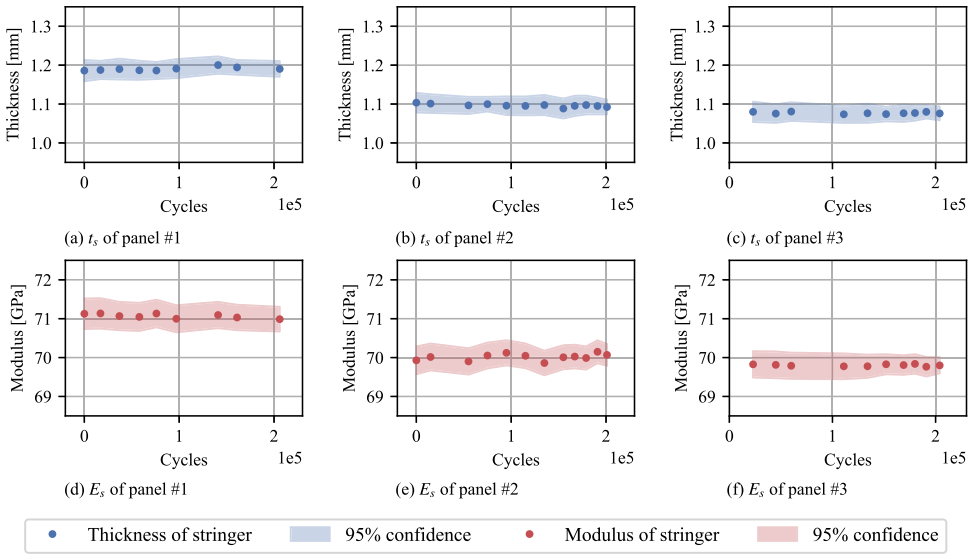

Fig. 12. Quantification of structural features of stringers during fatigue crack growth.

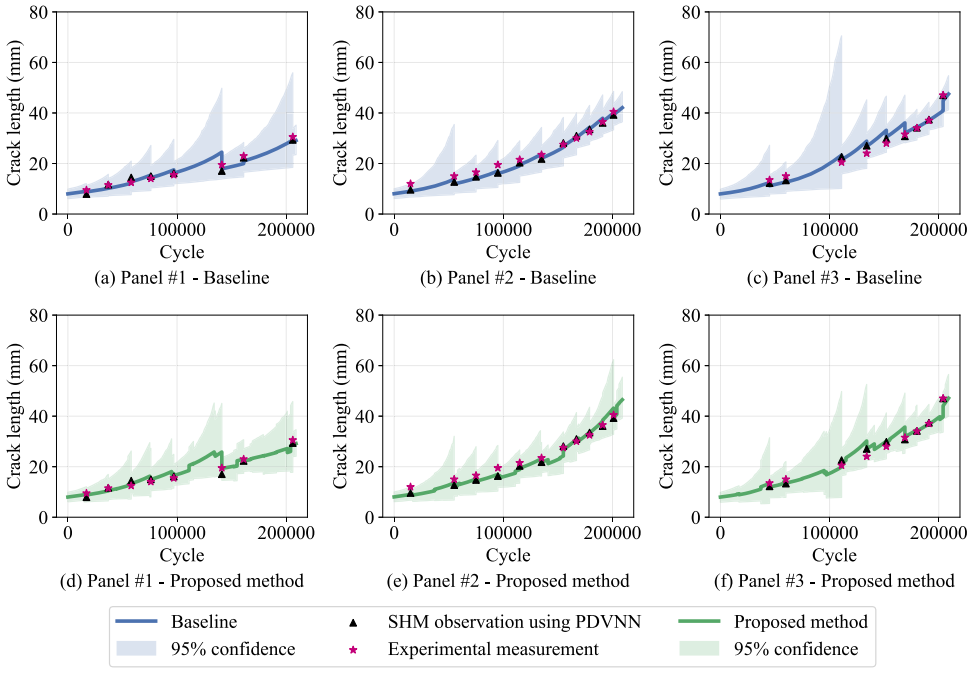

Fig. 13. Comparison of the damage diagnosis and prognosis.

$$R^2 = 1 - \frac{\sum_{i=1}^{n}\left(y_i - \hat{y}_i\right)^2}{\sum_{i=1}^{n}\left(y_i - \bar{y}\right)^2} \tag{23}$$

$$\mathrm{ABW} = \frac{1}{\mathrm{n}}\sum_{\mathrm{i}=1}^{\mathrm{n}}\left(\hat{y}_{\mathrm{i}}^{\mathrm{u}} - \hat{y}_{\mathrm{i}}^{\mathrm{l}}\right)^2 \tag{24}$$

where n is the number of data points; y_i and $\hat{y}_i$ are the observed and predicted values for the i_{th} sample, respectively, $\bar{y}$ is the mean of the observation, $\hat{y}_i^u$ and $\hat{y}_i^l$ represent the upper and lower bounds of 95 % confidence interval, respectively.

4. Results and discussion

In this section, the effectiveness of the proposed method, which integrates PDVNN and copula function for structural damage diagnosis and prognosis in a fleet, is evaluated. The performance of the proposed method is compared with existing methods using an experimental dataset from helicopter fuselage panels. Section 4.1 presents the results of damage state and structural feature quantification through the physical feature extraction model $\mathcal{M}^{\theta}$, which was developed based on the PDVNN. Section 4.2 provides a comparative analysis of the proposed method against existing methods, highlighting its superior performance in structural damage diagnosis and prognosis. To further demonstrate the applicability of the method to large datasets representative of real-world fleet scenarios, Section 4.3 presents a more comprehensive demonstration based on a hypothetical dataset comprising 36 samples.

4.1. Structural features and damage state quantification

Fig. 10 presents the quantified crack length results based on the SHM signals collected during the fatigue crack growth process. The measured

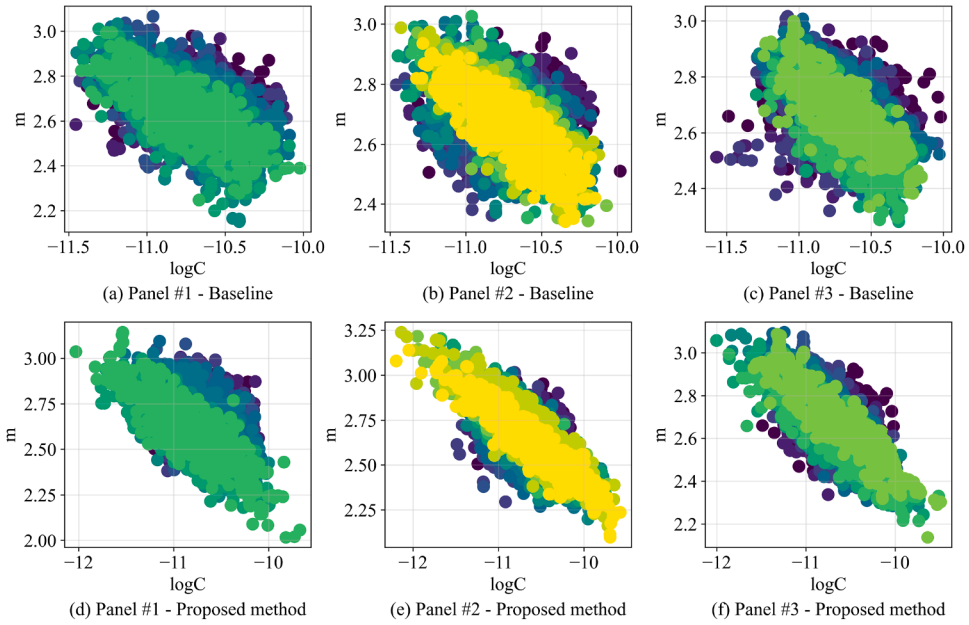

Fig. 14. Updating of crack growth parameters log$C$ and m.

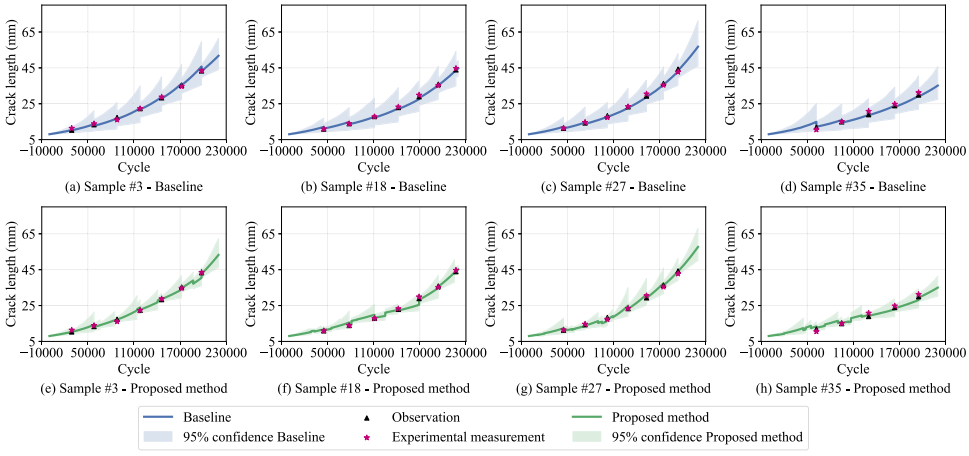

Fig. 15. Comparison of the damage diagnosis and prognosis of four typical samples.

crack lengths during the three tests closely align with the PDVNN model quantification, consistently falling within the 95 % confidence interval. These results highlight the effectiveness of the PDVNN model in accurately identifying structural damage while offering reliable uncertainty quantification.

Furthermore, Figs. 11 and 12 show the quantification results for the structural features of the three specimens, which have identical nominal dimensions and material properties for both the skin and stringer. Despite these similarities, the structural features extracted from the monitored signals indicate discrepancies in the thicknesses of the skins and stringers, as well as in the Young's modulus, compared to the nominal values. These variations in geometry and material properties were then incorporated into the structural similarity metrics and the collaborative damage diagnosis process for the fleet.

4.2. Comparison of the diagnosis and prognosis results

Building on the damage quantification results from Section 4.1, structural damage diagnosis and prognosis were performed using the methodology outlined in Section 2.4. Fig. 13 compares the proposed method with the conventional individual-based PF method.

As shown in Fig. 13, during the crack growth process for each specimen, for both methods, the PDVNN model extracts individual damage states and structural features when sensor monitoring signals are available, updating the model based on these states and reducing the uncertainty in the prediction results. However, compared to the baseline, the accuracy of crack diagnosis and the uncertainty associated with the crack growth process are significantly enhanced by the Copula-based update step incorporated into the proposed method. Notably, for panel #1 and panel #3, where monitoring data were missing for a period during crack growth, the collaborative updating method still effectively manages the uncertainty during this phase.

Table 4 presents the results of three evaluation metrics. The proposed method demonstrates lower prediction error, better model fitting, and reduced bandwidth compared to the baseline. Overall, prediction accuracy and goodness of fit improve by 11 %, while the overall uncertainty in the process is reduced by 8 %. It is important to note that the crack growth in panel #1 is significantly slower than in panels #2 and #3. This slower growth increases the signal-to-noise ratio of the observed data, which reduces the effectiveness of the observation-based updating. Furthermore, due to the differing damage growth in panels #2 and #3, the correlation between their damage states is lower, resulting in

Table 4
Comparison of prediction accuracy and uncertainty.

Specimen	Method	RMSE	R^2	ABW
Panel #1	Baseline	0.934	0.743	8.601
	Proposed method	**0.809**	**0.800**	**7.796**
Panel #2	Baseline	0.710	0.873	8.464
	Proposed method	**0.669**	**0.894**	**8.195**
Panel #3	Baseline	0.836	0.701	8.965
	Proposed method	**0.718**	**0.882**	**7.953**
Average	Baseline	0.827	0.772	8.677
	Proposed method	**0.732**	**0.858**	**7.981**

Table 5
Comparison of prediction accuracy and uncertainty.

Specimen	Method	RMSE	R^2	ABW
Sample #3	Baseline	0.459	0.947	7.269
	Proposed method	**0.373**	**0.965**	**3.558**
Sample #18	Baseline	0.567	0.920	7.629
	Proposed method	**0.461**	**0.945**	**3.375**
Sample #27	Baseline	0.561	0.921	7.551
	Proposed method	**0.440**	**0.952**	**4.117**
Sample #35	Baseline	0.521	0.909	7.757
	Proposed method	**0.475**	**0.944**	**3.725**
Average of all Samples	Baseline	0.521	0.932	7.417
	Proposed method	**0.449**	**0.950**	**3.615**

slightly less accurate updating for panel #1. Despite these challenges, the proposed method still outperforms the baseline in fleet diagnosis and prognosis.

Furthermore, the results of updating the crack growth model parameters are compared. As shown in Fig. 14, the updates of the material parameters $\log C$ and m using the proposed method outperform those from the conventional individual-based PF method. This highlights that the additional update step enhances the efficiency of the digital twin model's parameter updating. Overall, the uncertainty in the material parameters is significantly reduced following the crack size update. This reduction is more pronounced when the true damage state and structural features deviate more from the initial distribution, indicating that the proposed method effectively utilizes the additional information provided by the crack size update.

4.3. Demonstration on a large-scale hypothetical dataset representative of real-world fleet scenarios

Building on the encouraging results from the three experimental panels, the method was further assessed under fleet-scale conditions. In total, 36 panels were simulated to capture realistic operational variability. Variations in geometric dimensions, material properties, and crack growth model parameters were introduced to represent individual differences among fleet members.

Fig. 15 presents a comparison between the proposed method and the baseline for four representative samples. Consequently, not all samples are updated in the same loading cycle. Among all samples, sample #18 exhibited the most substantial reduction in uncertainty, whereas sample #27 achieved the largest reduction in RMSE but demonstrated relatively poorer uncertainty control. Samples #3 and #35 roughly represented the average level of performance improvement of the proposed method relative to the baseline.

As shown in Fig. 15, incorporating the Copula-based update step significantly reduces the uncertainty associated with crack growth, as quantified by the ABW values in Table 5.

In this demonstration, multiple observations were introduced with fewer cycles, which is generally advantageous for particle filtering methods. Nevertheless, as shown in Table 5, the proposed method consistently outperforms the baseline, improving both the accuracy of damage diagnosis and prognosis. Notably, it achieves a substantial reduction in prediction uncertainty, with ABW decreasing by more than 51 % on average. It should be noted, however, that this demonstration still needs to be extended to realistic datasets in our future study.

5. Conclusion

This study proposes a novel method for structural damage diagnosis and prognosis in a fleet of aircraft. The method leverages the PDVNN, which extracts individual damage states and structural features from sensor monitoring data while also capturing the correlations of damage states across different structures within the fleet. By incorporating the Copula function, the joint probability distribution of structural damage across two individual structures is established, enabling collaborative diagnosis and prognosis for multi-aircraft damage.

The effectiveness of the proposed method is validated through an aeronautical panel-based study. Compared to the conventional individual-based PF method, the proposed approach demonstrates superior accuracy and reliability in structural damage prediction. Specifically, the overall prediction accuracy and goodness-of-fit improve by 11 %, while the uncertainty in the process is reduced by 8 %.

Regarding scalability, the framework establishes separate digital twins for the crack growth of each fleet member, rather than a single integrated model for the entire fleet as in dynamic Bayesian networks. Feature extraction via PDVNN remains individual-oriented, while correlation modeling via Copula is decoupled from each individual's marginal distribution. Consequently, expanding to larger fleet sizes does not cause exponential growth in computational burden. In addition, collaborative updates are triggered selectively: if the correlation between two individuals falls below a predefined threshold, no update is performed. This design improves efficiency and prevents negative optimization in structural damage prediction.

In future work, the method needs to be validated on larger datasets and monitoring data from in-service structures to further assess prediction accuracy, robustness, and practical feasibility. Overall, these characteristics make the proposed framework a promising solution for scalable fleet-level structural damage diagnosis and prognosis, while highlighting the need for additional validation in complex real-world scenarios and the development of complementary inspection interval strategies.

CRediT authorship contribution statement

Jiaqi Xu: Writing – original draft, Software, Methodology, Formal analysis, Data curation; **Dingqiang Dai:** Visualization, Software, Methodology; **Xuan Zhou:** Writing – review & editing, Supervision, Methodology, Funding acquisition, Conceptualization; **Marco Giglio:** Writing – review & editing, Data curation; **Claudio Sbarufatti:** Writing – review & editing, Resources, Data curation; **Leiting Dong:** Writing – review & editing, Supervision, Project administration, Methodology, Funding acquisition.

Declaration of generative AI and AI-assisted technologies in the writing process

During the preparation of this work the authors used ChatGPT in the writing process in order to improve the readability and language of the manuscript. After using this tool, the authors reviewed and edited the content as needed and take full responsibility for the content of the published article.

Data availability

Data will be made available on request.

Declaration of competing interest

The authors declare that they have no known competing financial interests or personal relationships that could have appeared to influence the work reported in this paper.

Acknowledgment

The work of the first three authors and the sixth author were supported by the National Natural Science Foundation of China (Grant No. 52402510), National Natural Science Foundation of China - Joint Fund of Civil Aviation Research (Grant No. U2433213) and the “111 Center” (Program No. B18002). The third author was supported by the China Postdoctoral Science Foundation under Grant Numbers 2025T181120, 2025M774242.

Appendix A. Structural features sampling and parameter settings of hypothetical dataset

The sampling results of the 36 sets of specimens are presented in Table A.1. They remain consistent with the variation ranges of the four characteristic parameters specified in Table 1 of Section 3.2. Moreover, the crack growth model parameters ensure that the hypothetical crack propagation process stays close to the experimental data points.

The parameter setting of the demonstration on a large-scale hypothetical dataset are listed in Table A.2. Prior distribution of the structural features t_s, E_s, t_p, E_p is the same as that in Table 3.

Table A.1
Distribution range of structural features.

Series	t_p	t_s	E_p	E_s	$\log C$	m
1	0.81830	1.29630	73.19871	70.84567	−9.85692	2.39823
2	0.80332	1.32573	73.81730	69.61969	−9.89710	2.43202
3	0.81076	1.30207	73.42069	69.75894	−9.91163	2.47449
4	0.79683	1.31387	73.63781	70.43834	−9.92605	2.45689
5	0.81592	1.27672	74.01354	70.32397	−9.91245	2.47617
6	0.80672	1.27137	74.48106	70.06666	−9.90471	2.44752
7	0.79648	1.28861	73.77569	70.29582	−9.84893	2.41879
8	0.79090	1.32237	73.16365	69.86579	−9.91445	2.46824
9	0.80362	1.29096	74.07550	70.97955	−9.92622	2.51282
10	0.78348	1.28112	74.36096	70.03832	−9.85794	2.38728
11	0.78988	1.31816	74.26119	70.64225	−9.87986	2.44691
12	0.78024	1.30649	73.53515	70.68005	−9.88438	2.42881
13	0.81830	1.29630	73.19871	70.84567	−9.26342	2.04367
14	0.80332	1.32573	73.81730	69.61969	−9.30503	2.06655
15	0.81076	1.30207	73.42069	69.75894	−9.27780	2.06935
16	0.79683	1.31387	73.63781	70.43834	−9.26034	2.00890
17	0.81592	1.27672	74.01354	70.32397	−9.23775	1.99121
18	0.80672	1.27137	74.48106	70.06666	−9.18625	1.85948
19	0.79648	1.28861	73.77569	70.29582	−9.20560	1.93473
20	0.79090	1.32237	73.16365	69.86579	−9.15085	1.85698
21	0.80362	1.29096	74.07550	70.97955	−9.22417	1.97205
22	0.78348	1.28112	74.36096	70.03832	−9.20584	1.96675
23	0.78988	1.31816	74.26119	70.64225	−9.29453	2.05449
24	0.78024	1.30649	73.53515	70.68005	−9.21748	1.97627
25	0.81830	1.29630	73.19871	70.84567	−9.82090	2.42361
26	0.80332	1.32573	73.81730	69.61969	−9.75727	2.33071
27	0.81076	1.30207	73.42069	69.75894	−9.76467	2.34296
28	0.79683	1.31387	73.63781	70.43834	−9.72739	2.37231
29	0.81592	1.27672	74.01354	70.32397	−9.76994	2.41955
30	0.80672	1.27137	74.48106	70.06666	−9.82096	2.50046
31	0.79648	1.28861	73.77569	70.29582	−9.78642	2.39714
32	0.79090	1.32237	73.16365	69.86579	−9.69236	2.30572
33	0.80362	1.29096	74.07550	70.97955	−9.71642	2.29986
34	0.78348	1.28112	74.36096	70.03832	−9.75043	2.32440
35	0.78988	1.31816	74.26119	70.64225	−9.66527	2.22086
36	0.78024	1.30649	73.53515	70.68005	−9.75733	2.31812

Table A.2
Parameter setting for particle filter.

Parameters	Meaning	Value
a_0	Prior distribution of the initial half crack length	$N \sim (8.00, 1.00^2)$
$\log C_0$	Prior distribution of $\log C$	$N \sim (-9.56, 0.20^2)$
m_0	Prior distribution of m	$N \sim (2.27, 0.08^2)$
$\Delta\sigma$	Stress range	45
ω_a	Noise of the crack growth	$N \sim (-0.05^2/2, 0.05^2)$
ω_1	Noise in the evolution of $\log C$ and m	$N \sim (0, 0.01^2)$
ω_2	Noise in the evolution of t_s, E_s, t_p, E_p	$N \sim (0, 0.01^2)$
N_s	Number of particles	1000
ΔN	Increment of loading cycle	1000
θ_0	Hyperparameters for the correlation metric	20
d_0	Hyperparameters for the correlation metric	0.05

References

[1] L. Molent, B. Aktepe, Review of fatigue monitoring of agile military aircraft, Fatigue Fract. Eng. Mater. Struct. 23 (9) (2000) 767–785. https://doi.org/10.1046/j.1460-2695.2000.00330.x
[2] R. Wanhill, L. Molent, S. Barter, Milestone case histories in aircraft structural integrity, in: Reference Module in Materials Science and Materials Engineering, Elsevier, 2016, pp. 1–2. https://doi.org/10.1016/B978-0-12-803581-8.00847-X
[3] H. Lee, H. Cho, S. Park, Review of the F-16 individual aircraft tracking program, J. Aircr. 49 (5) (2012) 1398–1405. https://doi.org/10.2514/1.C031692
[4] Y. Liu, L. Wang, B.F. Ng, Multitask-transfer-learning method for random-force frequency identification considering multisource uncertainties, AIAA J. (2024) 1–16. https://doi.org/10.2514/1.J064860
[5] H.R. Golmakani, Condition-based inspection scheme for condition-based maintenance, Int. J. Prod. Res. 50 (14) (2012) 3920–3935. https://doi.org/10.1080/00207543.2011.611540
[6] R. Chen, S. Wang, C. Zhang, H. Dui, Y. Zhang, Y. Zhang, Y. Li, Component uncertainty importance measure in complex multi-state system considering epistemic uncertainties, Chin. J. Aeronaut. 37 (12) (2024) 31–54. https://doi.org/10.1016/j.cja.2024.05.024
[7] E.J. Tuegel, A.R. Ingraffea, T.G. Eason, S.M. Spottswood, Reengineering aircraft structural life prediction using a digital twin, Int. J. Aerosp. Eng. 2011 (2011) 1–14. https://doi.org/10.1155/2011/154798
[8] E. Glaessgen, D. Stargel, The digital twin paradigm for future NASA and U.S. air force vehicles, in: 53rd AIAA/ASME/ASCE/AHS/ASC Structures, Structural Dynamics and Materials Conference, American Institute of Aeronautics and Astronautics, Honolulu, Hawaii, 2012, p. 1818. https://doi.org/10.2514/6.2012-1818
[9] X. Qing, Y. Liao, Y. Wang, B. Chen, F. Zhang, Y. Wang, Machine learning based quantitative damage monitoring of composite structure, Int. J. Smart Nano Mater. 13 (2) (2022) 167–202. https://doi.org/10.1080/19475411.2022.2054878
[10] J. Chen, Y. Meng, Y. Xu, A multi-layer ML model evolutionary paradigm for high-accuracy individual aircraft SHM, Aerosp. Sci. Technol. 144 (2024) 108824. https://doi.org/10.1016/j.ast.2023.108824
[11] A. Thelen, X. Zhang, O. Fink, Y. Lu, S. Ghosh, B.D. Youn, M.D. Todd, S. Mahadevan, C. Hu, Z. Hu, A comprehensive review of digital twin — Part 1: modeling and twinning enabling technologies, Struct. Multidiscip. Optim. 65 (12) (2022) 354. https://doi.org/10.1007/s00158-022-03425-4
[12] A. Thelen, X. Zhang, O. Fink, Y. Lu, S. Ghosh, B.D. Youn, M.D. Todd, S. Mahadevan, C. Hu, Z. Hu, A comprehensive review of digital twin—Part 2: roles of uncertainty quantification and optimization, a battery digital twin, and perspectives, Struct. Multidiscip. Optim. 66 (1) (2023) 1. https://doi.org/10.1007/s00158-022-03410-x
[13] X. Zhou, S. He, L. Dong, S.N. Atluri, Real-time prediction of probabilistic crack growth with a helicopter component digital twin, AIAA J. 60 (4) (2022) 2555–2567. https://doi.org/10.2514/1.J060890
[14] F. Zhao, X. Zhou, C. Wang, L. Dong, S.N. Atluri, Setting adaptive inspection intervals in helicopter components, based on a digital twin, AIAA J. 61 (6) (2023) 2675–2688. https://doi.org/10.2514/1.J062222
[15] C. Zhang, Y. Lu, R. Chen, S. Wang, H. Dui, Y. Zhang, Y. Zhang, Resilience-based complex system early design using dynamic copula Bayesian network: heave compensation hydraulic system design as a case study, Ocean Eng. 320 (2025) 120314. https://doi.org/10.1016/j.oceaneng.2025.120314
[16] H.-K. Wang, R. Haynes, H.-Z. Huang, L. Dong, S.N. Atluri, The use of high-performance fatigue mechanics and the extended Kalman / particle filters, for diagnostics and prognostics of aircraft structures, CMES - Comput. Model. Eng. Sci. 105 (1) (2015) 1–24.
[17] C. Li, S. Mahadevan, Y. Ling, S. Choze, L. Wang, Dynamic Bayesian network for aircraft wing health monitoring digital twin, AIAA J. 55 (3) (2017) 930–941. https://doi.org/10.2514/1.J055201
[18] J. Chen, S. Yuan, H. Wang, On-line updating Gaussian process measurement model for crack prognosis using the particle filter, Mech. Syst. Signal Process. 140 (2020) 106646. https://doi.org/10.1016/j.ymssp.2020.106646
[19] T. Li, C. Sbarufatti, F. Cadini, J. Chen, S. Yuan, Particle filter-based hybrid damage prognosis considering measurement bias, Struct. Control Health Monit. 29 (4) (2022). https://doi.org/10.1002/stc.2914
[20] Y. Ye, Q. Yang, J. Zhang, S. Meng, J. Wang, X. Tang, A reconfigurable dynamic bayesian network for digital twin modeling of structures with multiple damage

modes, Theor. Appl. Mech. Lett. 13 (4) (2023) 100440. https://doi.org/10.1016/j.taml.2023.100440
[21] Y. Wang, M. He, L. Sun, D. Wu, Y. Wang, X. Qing, Weighted adaptive Kalman filtering-based diverse information fusion for hole edge crack monitoring, Mech. Syst. Signal Process. 167 (2022) 108534. https://doi.org/10.1016/j.ymssp.2021.108534
[22] J. Chen, S. Yuan, X. Jin, On-line prognosis of fatigue cracking via a regularized particle filter and guided wave monitoring, Mech. Syst. Signal Process. 131 (2019) 1–17. https://doi.org/10.1016/j.ymssp.2019.05.022
[23] D. Cristiani, C. Sbarufatti, F. Cadini, M. Giglio, Fatigue damage diagnosis and prognosis of an aeronautical structure based on surrogate modelling and particle filter, Struct. Health Monit. 20 (5) (2021) 2726–2746. https://doi.org/10.1177/1475921720971551
[24] L. Lin, B. Luo, S. Zhong, Multi-objective decision-making model based on CBM for an aircraft fleet with reliability constraint, Int. J. Prod. Res. 56 (14) (2018) 4831–4848. https://doi.org/10.1080/00207543.2018.1467574
[25] L. Colombo, D. Oboe, C. Sbarufatti, F. Cadini, S. Russo, M. Giglio, Shape sensing and damage identification with iFEM on a composite structure subjected to impact damage and non-trivial boundary conditions, Mech. Syst. Signal Process. 148 (2021) 107163. https://doi.org/10.1016/j.ymssp.2020.107163
[26] J. Xu, X. Zhou, M. Giglio, C. Sbarufatti, L. Dong, Variational neural network embedded with digital twins for probabilistic structural damage quantification, AIAA J. 63 (6) (2025) 2474–2486. https://doi.org/10.2514/1.J064808
[27] S. Jia, Y. Deng, J. Lv, S. Du, Z. Xie, Joint distribution adaptation with diverse feature aggregation: a new transfer learning framework for bearing diagnosis across different machines, Measurement 187 (2022) 110332. https://doi.org/10.1016/j.measurement.2021.110332
[28] M. Haugh, An introduction to copulas, in: IEOR E4602: Quantitative Risk Management, Columbia University, New York, USA, 2016, pp. 1–21.
[29] X. Zhang, H. Jiang, Application of copula function in financial risk analysis, Comput. Electr. Eng. 77 (2019) 376–388. https://doi.org/10.1016/j.compeleceng.2019.06.011
[30] C.R. Bhat, N. Eluru, A copula-based approach to accommodate residential self-selection effects in travel behavior modeling, Transp. Res. Part B Methodol. 43 (7) (2009) 749–765. https://doi.org/10.1016/j.trb.2009.02.001
[31] W. Huiyong, J. Shuchun, L. Hongkun, Y. Tongtong, Supply chain financing risk measurement of small and micro enterprises based on logistic-copula model, in: 2021 3rd International Conference on E-Business and E-Commerce Engineering, ACM, Sanya China, 2021, pp. 158–163. https://doi.org/10.1145/3510249.3510308
[32] G. Fang, R. Pan, Y. Hong, Copula-based reliability analysis of degrading systems with dependent failures, Reliab. Eng. Syst. Saf. 193 (2020) 106618. https://doi.org/10.1016/j.ress.2019.106618
[33] R. Chen, C. Zhang, S. Wang, E. Zio, H. Dui, Y. Zhang, Importance measures for critical components in complex system based on copula hierarchical Bayesian network, Reliab. Eng. Syst. Saf. 230 (2023) 108883. https://doi.org/10.1016/j.ress.2022.108883
[34] X. Liu, H. Lai, X. Wang, X. Song, K. Liu, S. Wu, Q. Li, F. Wang, Z. Zhou, Aerospace structural reliability analysis method based on regular vine copula model with the asymmetric tail correlation, Aerosp. Sci. Technol. 142 (2023) 108670. https://doi.org/10.1016/j.ast.2023.108670
[35] D.P. Kingma, M. Welling, Auto-encoding variational bayes, 2013. https://doi.org/10.48550/ARXIV.1312.6114
[36] E.W. Frees, E.A. Valdez, Understanding relationships using copulas, North Am. Actuarial J. 2 (1) (1998) 1–25. https://doi.org/10.1080/10920277.1998.10595667
[37] D.X. Li, On default correlation: a copula function approach, SSRN Electron. J. (1999). https://doi.org/10.2139/ssrn.187289
[38] S. Kullback, R.A. Leibler, On information and sufficiency, Ann. Math. Stat. 22 (1) (1951) 79–86. https://doi.org/10.1214/aoms/1177729694
[39] H. Mao, W. Tang, W. Zhu, G. Yang, X. Li, Z. Huang, H. Mao, B. Si, Feasibility study on wheelset fatigue damage with NOFRFs-KL divergence detection method in SIMO, J. Sound Vibr. 483 (2020) 115447. https://doi.org/10.1016/j.jsv.2020.115447
[40] R.B. Nelsen, Concordance, in: An Introduction to Copulas, Springer, 2006, pp. 138–179.
[41] D. Colombo, M. Giglio, A. Manes, 3D fatigue crack propagation analysis of a helicopter component, Int. J. Mater. Prod. Technol. 30 (1/2/3) (2007) 107. https://doi.org/10.1504/IJMPT.2007.013116
[42] C. Sbarufatti, A. Manes, M. Giglio, Application of sensor technologies for local and distributed structural health monitoring: Application of Sensor Technologies for Local and Distributed SHM, Struct. Control Health Monit. 21 (7) (2014) 1057–1083. https://doi.org/10.1002/stc.1632
[43] P. Paris, F. Erdogan, A critical analysis of crack propagation laws, J. Basic Eng. 85 (4) (1963) 528–533. https://doi.org/10.1115/1.3656900
[44] C.C. Poe, Stress Intensity Factor for a Cracked Sheet with Riveted and Uniformly Spaced Stringers, Technical Report L-6826, NASA Langley Research Center, Hampton, 1971.
[45] C. Sbarufatti, A. Manes, M. Giglio, Performance optimization of a diagnostic system based upon a simulated strain field for fatigue damage characterization, Mech. Syst. Signal Process. 40 (2) (2013) 667–690. https://doi.org/10.1016/j.ymssp.2013.06.003
[46] X. Zhou, C. Sbarufatti, M. Giglio, L. Dong, A fuzzy-set-based joint distribution adaptation method for regression and its application to online damage quantification for structural digital twin, Mech. Syst. Signal Process. 191 (2023) 110164. https://doi.org/10.1016/j.ymssp.2023.110164
[47] L. Xiong, M. Wan, X. Wei, K.M. O'Connor, Indices for assessing the prediction bounds of hydrological models and application by generalised likelihood uncertainty estimation / Indices Pour Évaluer Les Bornes de Prévision de Modèles Hydrologiques et Mise En Œuvre Pour Une Estimation d'incertitude Par Vraisemblance Généralisée, Hydrol. Sci. J. 54 (5) (2009) 852–871. https://doi.org/10.1623/hysj.54.5.852